

Time like geodesics in three-dimensional rotating Hořava AdS black hole

P. A. González*

*Facultad de Ingeniería y Ciencias, Universidad Diego Portales,
Avenida Ejército Libertador 441, Casilla 298-V, Santiago, Chile.*

Marco Olivares†

*Facultad de Ingeniería y Ciencias, Universidad Diego Portales,
Avenida Ejército Libertador 441, Casilla 298-V, Santiago, Chile.*

Eleftherios Papantonopoulos‡

Department of Physics, National Technical University of Athens, Zografou Campus GR 157 73, Athens, Greece.

Yerko Vásquez§

*Departamento de Física, Facultad de Ciencias,
Universidad de La Serena,
Avenida Cisternas 1200, La Serena, Chile.*

(Dated: August 4, 2020)

We study the motion of particles in the background of a three-dimensional rotating Hořava AdS black hole that corresponds to a Lorentz-violating version of the BTZ black hole and we analyze the effect of the breaking of Lorentz invariance in such motion by solving analytically the geodesic equations. Mainly, we find that Lorentz-violating version of the BTZ black hole posses a more rich geodesic structure, where the planetary and circular orbits are allowed, which does not occurs in the BTZ background.

PACS numbers:

Keywords:

Contents

I. Introduction	2
II. Three-dimensional rotating Hořava black holes	2
III. Equations of motion	5
IV. Time like geodesics	6
A. Planetary orbit	7
B. Circular orbits	10
C. Critical trajectories	11
D. Radial motion	14
V. Remarks and conclusions	15
Acknowledgments	16
References	16

*Electronic address: pablo.gonzalez@udp.cl

†Electronic address: marco.olivares@mail.udp.cl

‡Electronic address: lpapa@central.ntua.gr

§Electronic address: yvasquez@userena.cl

I. INTRODUCTION

The three-dimensional models of gravity are of interest because it is possible to investigate efficiently some of their properties which are shared by their higher dimensional analogs, and also exhibit interesting solutions such as particle-like solutions and black holes. In this context, three-dimensional general relativity (GR), which has no local gravitational degrees of freedom, and is Lorentz invariant presents the well know Bañados–Teitelboim–Zanelli (BTZ) black hole solution with a negative cosmological constant [1]. Also, it presents interesting properties at both classical and quantum levels and the BTZ solution shares several features of the Kerr black hole [2]. An important issue in gravitational physics is to know the kind of orbits that test particles follow outside the event horizon of a black hole. This information can be provided by studying the geodesics around these black holes, in this context for the BTZ background it was shown that while massive particles always fall into the event horizon and no stable orbits are possible [3], massless particles can escape or plunge to the horizon [4].

The three-dimensional Hořava gravity [5] admits a Lorentz-violating version of the BTZ black hole, i.e. a black hole solution with AdS asymptotics, only in the sector of the theory in which the scalar degree of freedom propagates infinitely fast [6]. Remarkably, in contrast to GR, the three-dimensional Hořava gravity also admits black holes with positive and vanishing cosmological constant. Nowadays, one could think that Lorentz invariance may not be fundamental or exact, but is merely an emergent symmetry on sufficiently large distances or low energies. It has been suggested in Ref. [7] that giving up Lorentz invariance by introducing a preferred foliation and terms that contain higher-order spatial derivatives can lead to significantly improved UV behavior, the corresponding gravity theory is dubbed Hořava gravity. It was shown that the propagation of massive scalar fields is stable in the background of rotating three-dimensional Hořava AdS black holes and by employing the holographic principle the different relaxation times of the perturbed system to reach thermal equilibrium were found for the various branches of solutions [8]. Also, concerning to the collision of particles, it was shown that the particles can collide on the inner horizon with arbitrarily high CM energy if one of the particles has a critical angular momentum being possible the BSW process, for the non-extremal rotating Hořava AdS black hole. Also, while that for the extremal BTZ black hole the particles with critical angular momentum only can exist on the degenerate horizon, for the Lorentz-violating version of the BTZ black hole the particle with critical angular momentum can exist in a region from the degenerate horizon [9]. Concerning to the null geodesics, it was shown that for the motion of photons new kinds of orbits are allowed, such as unstable circular orbits and trajectories of first kind. Also, it was shown that an external observer will see that photons arrive at spatial infinity in a finite coordinate time [10].

In this work we study the motion of particles in the background of a three-dimensional rotating Hořava AdS black hole [6], with the aim of analyzing the effect of breaking the Lorentz symmetry by calculating the time like geodesic structure. We will show that Lorentz-violating version of the BTZ black hole posses a more rich geodesic structure, where the planetary orbits are allowed, which does not occur in the BTZ background. Also, we will have a complete knowledge of the geodesic structure for the rotating three-dimensional Hořava AdS black hole allowing us to understand in depth the Lorentz-violating effects on the BTZ black hole. For other studies about geodesics in three-dimensional spacetimes, see [11–14].

The work is organized as follows. In Sec. II we give a brief review of three-dimensional rotating Hořava AdS black hole. In Sec. III we find the motion equations for particles and we present the time like geodesic structure in Sec. IV. Finally, our conclusions are in Sec. V.

II. THREE-DIMENSIONAL ROTATING HOŘAVA BLACK HOLES

The three-dimensional Hořava gravity is described in a preferred foliation by the action [5]

$$S_H = \frac{1}{16\pi G_H} \int dT d^2x N \sqrt{g} [L_2 + L_4], \quad (1)$$

being the line element in the preferred foliation

$$ds^2 = N^2 dT^2 - g_{ij}(dx^i + N^i dT)(dx^j + N^j dT), \quad (2)$$

where g_{ij} is the induced metric on the constant- T hypersurfaces. G_H is a coupling constant with dimensions of a length squared, g is the determinant of g_{ij} and the Lagrangian L_2 has the following form

$$L_2 = K_{ij}K^{ij} - \lambda K^2 + \xi \left({}^{(2)}R - 2\Lambda \right) + \eta a_i a^i, \quad (3)$$

where K_{ij} , K , and ${}^{(2)}R$ correspond to extrinsic, mean, and scalar curvature, respectively, and a_i is a parameter related to the lapse function N via $a_i = -\partial_i \ln N$. L_4 corresponds to the set of all the terms with four spatial derivatives that are invariant under diffeomorphisms. For $\lambda = \xi = 1$ and $\eta = 0$, the action reduces to that of general relativity. In the infrared limit of the theory the higher order terms L_4 (UV regime) can be neglected, and the theory is equivalent to a restricted version of the Einstein-aether theory, the equivalence can be showed by restricting the aether to be hypersurface-orthogonal and the following relation is obtained

$$u_\alpha = \frac{\partial_\alpha T}{\sqrt{g^{\mu\nu} \partial_\mu T \partial_\nu T}}, \quad (4)$$

where u_α is a unit-norm vector field called the aether, see Ref. [15] for details. Another important characteristic of this theory is that only in the sector $\eta = 0$, Hořava gravity admits asymptotically AdS solutions [6]. Therefore, assuming stationary and circular symmetry the most general metric is given by

$$ds^2 = Z(r)^2 dt^2 - \frac{1}{F(r)^2} dr^2 - r^2 (d\phi + \Omega(r) dt)^2, \quad (5)$$

and by assuming the aether to be hypersurface-orthogonal, it results

$$u_t = \pm \sqrt{Z(r)^2 (1 + F^2(r) U^2(r))}, u_r = U(r). \quad (6)$$

The theory admits the BTZ “analogue” to the three-dimensional rotating Hořava black holes described by the solution

$$F(r)^2 = Z(r)^2 = -M + \frac{\bar{J}^2}{4r^2} - \bar{\Lambda} r^2, \quad \Omega(r) = -\frac{J}{2r^2}, \quad U(r) = \frac{1}{F(r)} \left(\frac{a}{r} + br \right), \quad (7)$$

where

$$\bar{J}^2 = \frac{J^2 + 4a^2(1 - \xi)}{\xi}, \quad \bar{\Lambda} = \Lambda - \frac{b^2(2\lambda - \xi - 1)}{\xi}. \quad (8)$$

The sign of the effective cosmological constant $\bar{\Lambda}$ determines the asymptotic behavior (flat, dS, or AdS) of the metric. Also, \bar{J}^2 can be negative, this occurs when either $\xi < 0$ or $\xi > 1$, $a^2 > J^2/(4(\xi - 1))$. The aether configuration for this metric is given explicitly by

$$u_t = \sqrt{F^2 + \left(\frac{a}{r} + br \right)^2}, \quad u_r = \frac{1}{F^2} \left(\frac{a}{r} + br \right), \quad u_\phi = 0, \quad (9)$$

where a and b are constants that can be regarded as measures of aether misalignment, with b as a measure of asymptotically misalignment, such that for $b \neq 0$ the aether does not align with the timelike Killing vector asymptotically. Note that for $\xi = 1$ and $\lambda = 1$, the solution becomes the BTZ black hole, and for $\xi = 1$ and $\lambda \neq 1$, the solution becomes the BTZ black hole with a shifted cosmological constant $\bar{\Lambda} = \Lambda - 2b^2(\lambda - 1)$. However, there is still a preferred direction represented by the aether vector field which breaks Lorentz invariance for $\lambda \neq 1$ and $b \neq 0$. The locations of the inner and outer horizons $r = r_\pm$, are given by

$$r_\pm^2 = -\frac{M}{2\bar{\Lambda}} \left(1 \pm \sqrt{1 + \frac{\bar{J}^2 \bar{\Lambda}}{M^2}} \right). \quad (10)$$

Besides the existence of inner and outer horizons, also there are universal horizons, which are given by [6]

$$(r_u^\pm)^2 = \frac{M - 2ab}{2(b^2 - \bar{\Lambda})} \pm \frac{1}{2(b^2 - \lambda)} [(M - 2ab)^2 - (4a^2 + \bar{J}^2)(b^2 - \bar{\Lambda})]^{1/2}. \quad (11)$$

The Fig. (1), show the behavior of the horizons as a function of the parameter b , and as a function of a in Fig. (2), for a choice of parameters. There are different zones, one of them is limited by r_- and r_+ ; and it is described by the existence of the aether, where the roots r_u^\pm are imaginary and therefore there are no universal horizons. Other zones are characterized by two real and distinct universal horizons inside the region between r_- and r_+ , outside r_- , and inside r_+ ; and an especial zone where both universal horizons coincide and is given by

$$r_u^2 = \frac{M - 2a_\pm(M, \bar{J}, b)b}{2(b^2 - \bar{\Lambda}(b))}, \quad (12)$$

where a_{\pm} are the roots of

$$\frac{(4a^2 + \bar{J}^2)(b^2 - \bar{\Lambda}(b))}{\xi(M - 2ab)^2} = 1. \quad (13)$$

In the region between r_u^- and r_u^+ , the aether turns imaginary and the foliation cannot be extended until the singularity.

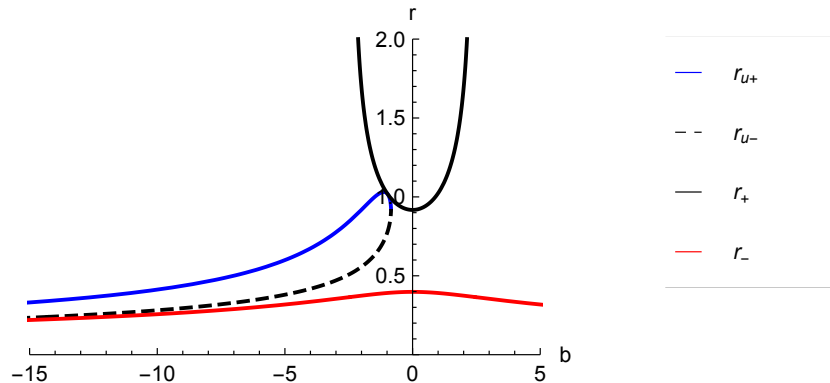


FIG. 1: The behavior of the horizons as a function of the parameter b , with $M = 1$, $\xi = 1.2$, $\lambda = 1$, $a = 1$, $\Lambda = -1$, and $J = 1.2$. For $b \approx -0.84$, $r_u^+ = r_u^-$ [9].

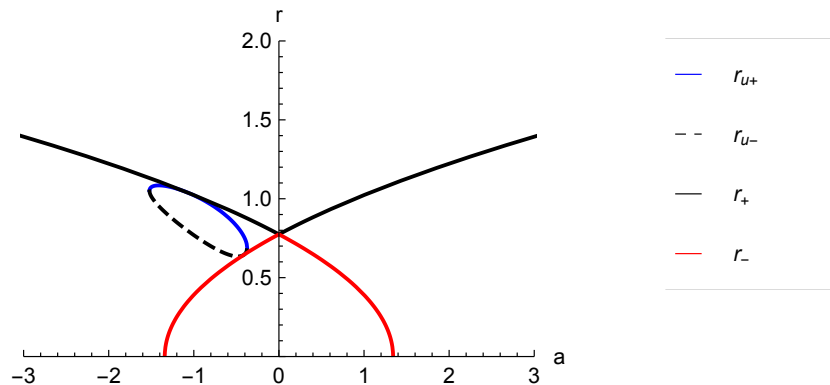


FIG. 2: The behavior of the horizons as a function of the parameter a , with $M = 1$, $\xi = 1.2$, $\lambda = 1$, $b = 1$, $\Lambda = -1$, and $J = 1.2$. For $a \approx -1.52$, and -0.37 , $r_u^+ = r_u^-$ [9].

In the following, we consider the zone limited by r_- and r_+ , which is described by the existence of the aether, where the roots r_u^{\pm} are imaginary and therefore there are no universal horizons.

III. EQUATIONS OF MOTION

In this section, we find the motion equations of probe massive particles around the three-dimensional Hořava AdS black hole. It is important to emphasize [16] that in a Lorentz-violating scenario, particles will be generically coupled to the aether field generating UV modifications of the matter dispersion relations, it is more, one can also expect radiative corrections in the infrared sector but these contributions are suppressed by known mechanisms. In our analysis we are interested on the infrared limit of the theory; so the presence of higher-order terms (L_4) related to the UV behaviour of the theory are ignored and in this case the theory can be formulated in a covariant fashion, and it then becomes equivalent to a restricted version of Einstein-aether theory [6]. Since our analysis is focused in the low energy part of the theory, the interaction between the massive particle and the aether field is ignored, thus the presence of aether field only affect the background spacetime geometry. It is worth mentioning that a similar analysis was performed in [17] where the authors analyzed the evolution of the photon around the static neutral and charged aether black holes using the Hamilton-Jacobi equation. Therefore, the massive particles follow the typical geodesics in such given black holes spacetime, that can be derived from the Lagrangian of a test particle, which is given by [18]

$$\mathcal{L} = \frac{1}{2} \left(g_{\mu\nu} \frac{dx^\mu}{d\tau} \frac{dx^\nu}{d\tau} \right). \quad (14)$$

So, for the three-dimensional rotating Hořava AdS black hole described by the metric (5), the Lagrangian associated with the motion of the test particles is given by

$$2\mathcal{L} = -[\mathcal{F}(r) - r^2\Omega^2(r)]\dot{t}^2 + 2r^2\Omega(r)\dot{t}\dot{\phi} + \frac{\dot{r}^2}{\mathcal{F}(r)} + r^2\dot{\phi}^2, \quad (15)$$

where $\dot{q} = dq/d\tau$, and τ is an affine parameter along the geodesic. Here, we have defined $F(r)^2 = Z(r)^2 = \mathcal{F}(r)$. Since the Lagrangian (15) is independent of the cyclic coordinates (t, ϕ) , then their conjugate momenta (Π_t, Π_ϕ) are conserved. Then, the equations of motion are obtained from $\dot{\Pi}_q - \frac{\partial \mathcal{L}}{\partial q} = 0$, and yield

$$\dot{\Pi}_t = 0, \quad \dot{\Pi}_r = -[\mathcal{F}'(r)/2 - r\Omega^2(r) - r^2\Omega'(r)]\dot{t}^2 - \frac{\mathcal{F}'(r)\dot{r}^2}{2\mathcal{F}^2(r)} + r\dot{\phi}^2, \quad \text{and} \quad \dot{\Pi}_\phi = 0, \quad (16)$$

where $\Pi_q = \partial \mathcal{L} / \partial \dot{q}$ are the conjugate momenta to the coordinate q , and are given by

$$\Pi_t = -[\mathcal{F}(r) - r^2\Omega^2(r)]\dot{t} + r^2\Omega(r)\dot{\phi} \equiv -E, \quad \Pi_r = \frac{\dot{r}}{\mathcal{F}(r)} \quad \text{and} \quad \Pi_\phi = r^2\Omega(r)\dot{t} + r^2\dot{\phi} \equiv L, \quad (17)$$

where E and L are integration constants associated to each of them. Therefore, the Hamiltonian is given by

$$\mathcal{H} = \Pi_t \dot{t} + \Pi_\phi \dot{\phi} + \Pi_r \dot{r} - \mathcal{L}. \quad (18)$$

Thus,

$$2\mathcal{H} = -E\dot{t} + L\dot{\phi} + \frac{\dot{r}}{\mathcal{F}(r)} \equiv -m^2. \quad (19)$$

where $m = 1$ for timelike geodesics or $m = 0$ for null geodesics. Therefore, we obtain

$$\dot{\phi} = -\frac{1}{(r^2 - r_+^2)(r^2 - r_-^2)\bar{\Lambda}} \left[\frac{EJ}{2} + L \left(-\bar{\Lambda}r^2 - M - \frac{J^2 - \bar{J}^2}{4r^2} \right) \right], \quad (20)$$

$$\dot{t} = -\frac{[Er^2 - JL/2]}{(r^2 - r_+^2)(r^2 - r_-^2)\bar{\Lambda}}, \quad (21)$$

$$r^2 = \left(E - \frac{JL}{2r^2} \right)^2 - \left(-M + \frac{\bar{J}^2}{4r^2} - \bar{\Lambda}r^2 \right) \left(m^2 + \frac{L^2}{r^2} \right) = (E - V_-)(E - V_+), \quad (22)$$

where $V_\pm(r)$ is the effective potential and it is given by

$$V_\pm(r) = \frac{JL}{2r^2} \pm \sqrt{\left(-M + \frac{\bar{J}^2}{4r^2} - \bar{\Lambda}r^2 \right) \left(m^2 + \frac{L^2}{r^2} \right)}. \quad (23)$$

Since the negative branches have no classical interpretation, they are associated with antiparticles in the framework of quantum field theory [19]. We choose the positive branch of the effective potential $V = V_+$. In the next section we will perform a general analysis of the equations of motion.

IV. TIME LIKE GEODESICS

In this section we analyze the motion of particles, $m^2 = 1$, so the effective potential is given by

$$V(r) = \frac{JL}{2r^2} + \sqrt{\left(-M + \frac{\bar{J}^2}{4r^2} - \bar{\Lambda}r^2\right) \left(1 + \frac{L^2}{r^2}\right)}, \quad (24)$$

whose behavior is showed in Fig. 3 for $J > 0$, and positive values of the angular momentum of the particle. Note that, for $L = 0$ the trajectory always have a turning point, from which the particle plunge in the event horizon, knowing as trajectory of second kind. Then, there is a critical value of the angular momentum (L_C) where the last stable circular orbit (LSCO) is present at $r = r_{LSCO}$; and for $L > L_C$ we can distinguish four orbits, the planetary, the second kind, the circular unstable at $r = r_U$, the circular stable at $r = r_S$, and critical orbits are allowed. Note that, these orbits does not occur in the BTZ background.

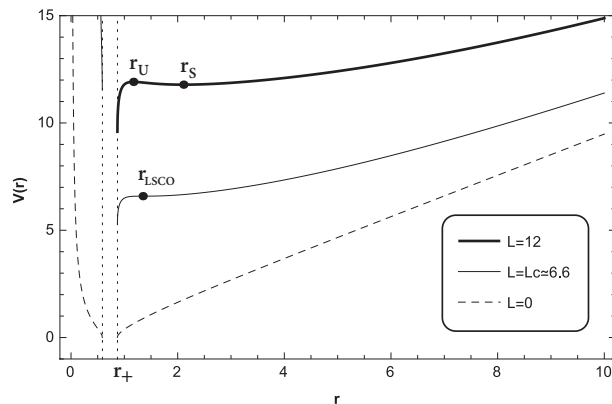


FIG. 3: The behavior of $V(r)$ as a function of r , for different values of the angular momentum of the particle L , with $M = a = b = \lambda = 1$, $\xi = 1.1$, $J = 1.2$, $r_+ \approx 0.87$ and $\Lambda = -1$.

The orbit in polar coordinates is given by

$$-\frac{r^2}{(r^2 - r_+^2)(r^2 - r_-^2)\bar{\Lambda}} \left[\frac{EJ}{2} + L \left(-\bar{\Lambda}r^2 - M - \frac{J^2 - \bar{J}^2}{4r^2} \right) \right] \left(\pm \frac{dr}{d\phi} \right) = \sqrt{P(r)}. \quad (25)$$

where we have used Eq. (20) and Eq. (22), $P(r)$ corresponds to the characteristic polynomial, and it is given by

$$\begin{aligned} P(r) &= r^6 \bar{\Lambda} + r^4 (E^2 + L^2 \bar{\Lambda} + M) + r^2 (L^2 M - JEL - \bar{J}^2/4) + (J^2 - \bar{J}^2)L^2/4 \\ P(r) &\equiv -\bar{\Lambda} (-r^6 + \alpha r^4 + \beta r^2 + \gamma). \end{aligned} \quad (26)$$

where

$$\alpha = -\frac{E^2 + M + \bar{\Lambda}L^2}{\bar{\Lambda}}, \quad (27)$$

$$\beta = \frac{JEL + \bar{J}^2/4 - ML^2}{\bar{\Lambda}}, \quad (28)$$

$$\gamma = -\frac{(J^2 - \bar{J}^2)L^2}{4\bar{\Lambda}}, \quad (29)$$

Therefore, we can see that depending on the nature of its roots, we can obtain the allowed motions for this spacetime.

A. Planetary orbit

The roots of $P(r) = 0$ allows to define the distance r_P , which corresponds to a *periastra* distance at the trajectory, r_A which is interpreted as a *apoastro* distance, and the distance r_F that represent the turning point for the trajectory, see Fig. 4. Thereby, planetary orbits of the first kind occur when $L > L_C$, and the energy E lies in the range $E_S < E < E_U$, so the radial coordinate will be $r_p < r < r_A$ for a certain value of E ; and the planetary orbits of the second kind occurs when $E < E_U$, and $r_H < r < r_F$.

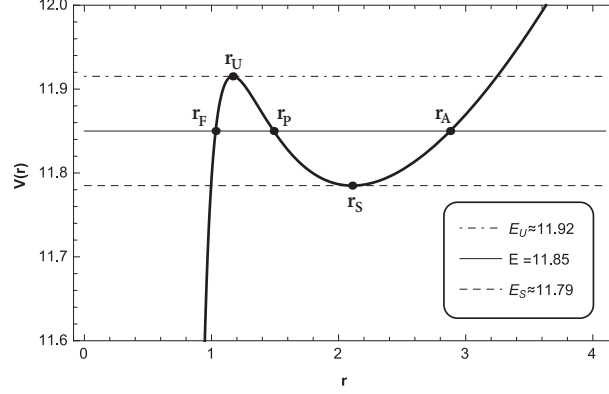


FIG. 4: The behavior of $V(r)$ as a function of r , for $L = 12$, $M = a = b = \lambda = 1$, $J = 1.2$, $\xi = 1.1$, $r_F \approx 1.03$, $r_U \approx 1.17$, $r_P \approx 1.49$, $r_S \approx 2.11$, $r_A \approx 2.88$, $E = 11.85$, $E_S = 11.79$, $E_U = 11.92$, and $\Lambda = -1$.

Thus, the characteristic polynomial (26) can be written as

$$P(r) = -\bar{\Lambda} (r_A^2 - r^2) (r^2 - r_P^2) (r^2 - r_F^2), \quad (30)$$

where

$$r_A = \left(\frac{\alpha}{3} + 2\sqrt{\frac{A}{3}} \cos \left[\frac{1}{3} \cos^{-1} \left[\frac{3B}{2} \sqrt{\frac{3}{A^3}} \right] \right] \right)^{1/2}, \quad (31)$$

$$r_P = \left(\frac{\alpha}{3} + 2\sqrt{\frac{A}{3}} \cos \left[\frac{1}{3} \cos^{-1} \left[\frac{3B}{2} \sqrt{\frac{3}{A^3}} \right] + \frac{4\pi}{3} \right] \right)^{1/2} \quad (32)$$

and

$$r_F = \left(\frac{\alpha}{3} + 2\sqrt{\frac{A}{3}} \cos \left[\frac{1}{3} \cos^{-1} \left[\frac{3B}{2} \sqrt{\frac{3}{A^3}} \right] + \frac{2\pi}{3} \right] \right)^{1/2} \quad (33)$$

where $A = \frac{\alpha^2}{3} + \beta$ and $B = \frac{2\alpha^3}{27} + \frac{\alpha\beta}{3} + \gamma$. Now, we will determine the angular coordinate of the trajectory for a particle that start at $r = r_A$, and it is given by the solution of the integral

$$\phi(r) = - \int_{r_A}^r \frac{r^2}{(-\bar{\Lambda})(r^2 - r_+^2)(r^2 - r_-^2)} \left[-L\bar{\Lambda}r^2 + \left(\frac{EJ}{2} - ML \right) - L \frac{J^2 - \bar{J}^2}{4r^2} \right] \frac{dr}{\sqrt{P(r)}}, \quad (34)$$

where we have used Eqs. (20) and (22), and whose solution is

$$\phi(r) = k_0 \Psi_0(r) + K_0 [k_+ \Psi_+(r) - k_- \Psi_-(r)], \quad (35)$$

where

$$k_0 = \frac{r_A L (J^2 - \bar{J}^2)}{8(-\bar{\Lambda})^{3/2} \sqrt{\gamma} r_+^2 r_-^2}, \quad \Psi_0(r) = \wp^{-1} [U(r_A)] - \wp^{-1} [U(r)], \quad (36)$$

$$k_{\pm} = \frac{EJ/2 - LM}{r_{\pm}^2} - \bar{\Lambda}L - \frac{L(J^2 - \bar{J}^2)}{4r_{\pm}^4}. \quad (37)$$

This solution is plotted in Fig. 5, where we can observe the trajectory of first and second kind. Note that, the coordinate (ϕ) diverges at the event horizon. Also, the solution (35) allow us to determine the precession angle, by considering that it is given by $\Theta = 2\phi_P - 2\pi$, where ϕ_P is the angle from the apoastro to the periastro. Thus, we obtain

$$\Theta = 2k_0 \Psi_0(r_P) + 2K_0 [k_+ \Psi_+(r_P) - k_- \Psi_-(r_P)] - 2\pi. \quad (38)$$

This is an exact solution for the angle of precession, and it depends on the spacetime parameters; M , J , \bar{J} , and the particles motion constants, E and L .

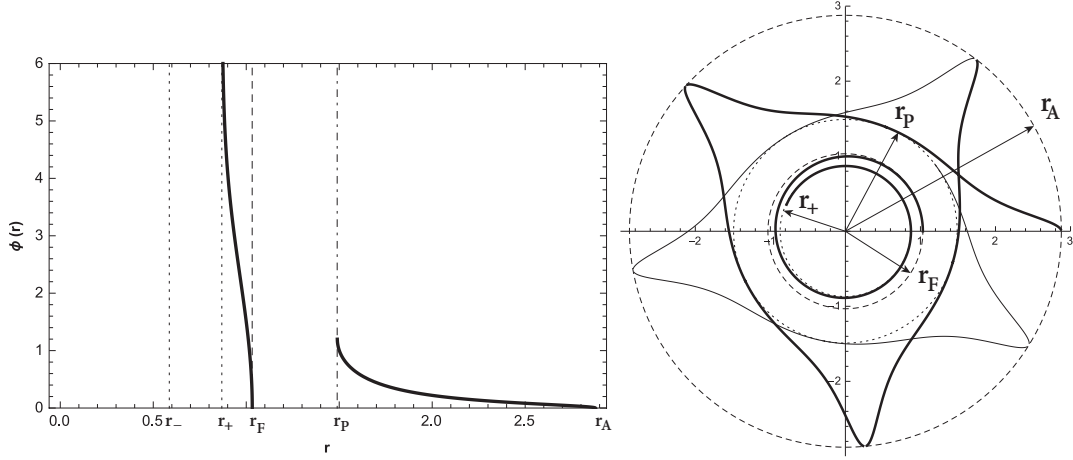


FIG. 5: The behaviour of $\phi(r)$ (left panel), and $r(\phi)$ (right panel) for bounded orbits of first and second kind with $E = 11.85$, $L = 12$, $M = a = b = \lambda = 1$, $\Lambda = -1$, $J = 1.2$, and $\xi = 1.1$.

Now, in order to determine the proper and coordinate period of rotation of the trajectories we present the solution for both times. The proper time (τ), is given by the solution of the integral

$$\tau(r) = - \int_{r_A}^r \frac{r^2 dr}{\sqrt{P(r)}}, \quad (39)$$

where we have used Eq. (22) and we have considered as initial conditions that the particles are at $r = r_A$ when $\phi = t = \tau = 0$. Thus, we obtain

$$\tau(r) = \frac{r_A^3}{8\sqrt{(-\Lambda)\gamma}} (\Psi[U(r), \Omega] - \Psi[U(r_A), \Omega]), \quad (40)$$

where

$$\Psi(U, \Omega) = \frac{1}{\wp'(\Omega)} \left[\zeta(\Omega) \wp^{-1}(U) + \ln \left| \frac{\sigma[\wp^{-1}(U) - \Omega]}{\sigma[\wp^{-1}(U) + \Omega]} \right| \right], \quad (41)$$

and

$$U(r) = \frac{r_A^2}{4r^2} + \frac{\beta r_A^2}{12\gamma}, \quad U(r_A) = \frac{1}{4} + \frac{\beta r_A^2}{12\gamma}, \quad (42)$$

$$\Omega = \wp^{-1} \left[\frac{\beta r_A^2}{12\gamma} \right], \quad (43)$$

$$g_2 = \frac{r_A^4}{4} \left[\frac{\beta^2}{3\gamma^2} - \frac{\alpha}{\gamma} \right], \quad g_3 = \frac{r_A^6}{16} \left[\frac{\alpha\beta}{3\gamma^2} - \frac{2\beta^3}{27\gamma^3} + \frac{1}{\gamma} \right]. \quad (44)$$

In Fig. 6, we show the behaviour of the proper time as a function of r , we can observe, for the trajectory of first and second kind the particle arrives in a finite time to r_P , and r_+ , respectively. Also, the period of a revolution according to the proper time is $T_\tau = 2\tau(r_P)$.

On the other hand, by considering Eqs. (21) and (22), and as initial condition that the particles are at $r = r_A$ when $\phi = t = \tau = 0$. The coordinate time (t) is

$$t(r) = - \int_{r_A}^r \frac{r^2 [Er^2 - JL/2]}{(-\bar{\Lambda})(r^2 - r_+^2)(r^2 - r_-^2) \sqrt{P(r)}} dr, \quad (45)$$

whose solution is

$$t(r) = K_0 \left[\left(E - \frac{JL}{2r_+^2} \right) \Psi_+(r) - \left(E - \frac{JL}{2r_-^2} \right) \Psi_-(r) \right], \quad (46)$$

where $K_0 = \frac{r_A^3}{8(-\bar{\Lambda})^{3/2} \sqrt{\gamma}(r_+^2 - r_-^2)}$, and

$$\Psi_\pm(r) = \Psi[U(r_A), \Omega_\pm] - \Psi[U(r), \Omega_\pm], \quad \Omega_\pm(r) = \wp^{-1} \left[\frac{r_A^2}{4r_\pm^2} + \frac{\beta r_A^2}{12\gamma} \right]. \quad (47)$$

In Fig. 6, we show the behaviour of the proper and coordinate time as a function of r , we can observe, for the trajectory of first and second kind the particle arrives in a finite proper time and infinity coordinate time to r_P , and r_+ , respectively. Also, the period of a revolution according to the coordinate time is $T_t = 2t(r_P)$.

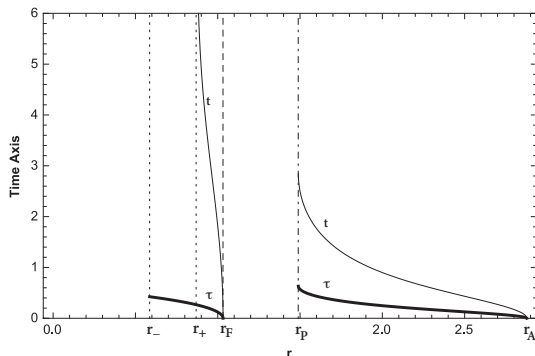


FIG. 6: The behaviour of the coordinate time (t) and the proper time (τ) along an bounded time-like geodesic described by a test particle, starting at $r_A = 2.88$, and $r_F = 1.03$ with $r_P = 1.49$, $L = 12$, $M = a = b = \lambda = 1$, $\Lambda = -1$, $E = 11.85$, $J = 1.2$, $\xi = 1.1$, $r_+ \approx 0.87$, and $r_- \approx 0.59$.

B. Circular orbits

The effective potential $V(r)$ has to exhibit extremes for fixed values of radial coordinate, $r = r_{c.o.}$, when

$$\left. \frac{dV(r)}{dr} \right|_{r_{c.o.}} = 0. \quad (48)$$

Now, for simplicity, we write the effective potential as

$$V(r) = \frac{JL}{2r^2} + \sqrt{\mathcal{F}(r) + L^2 \frac{\mathcal{F}(r)}{r^2}}. \quad (49)$$

Therefore, using Eq. (49) into Eq. (48) yields

$$\left[r^3 \mathcal{F}'(r) + L^2 [r \mathcal{F}'(r) - 2\mathcal{F}(r)] - 2JL \sqrt{\mathcal{F}(r) + L^2 \frac{\mathcal{F}(r)}{r^2}} \right] \Big|_{r_{c.o.}} = 0. \quad (50)$$

Notice that this equation leads to a polynomial of twelfth grade, so, it is possible to find the roots numerically. The condition (50) allows to obtain the angular momentum for the stable $L_{c.o.} = L_S$ at $r_{c.o.} = r_S$ (LSCO) and for the unstable circular orbits $L_{c.o.} = L_U$ at $r_{c.o.} = r_U$, which yields

$$\mathcal{A} L_{c.o.}^4 - \mathcal{B} L_{c.o.}^2 + \mathcal{C} = 0, \quad (51)$$

where

$$\begin{aligned} \mathcal{A} &= \left[4(M^2 + \bar{\Lambda} J^2) + (J^2 - \bar{J}^2) \left(\frac{4M}{r^2} - \frac{\bar{J}^2}{r^4} \right) \right] \Big|_{r_{c.o.}}, \\ \mathcal{B} &= \left[\frac{\bar{J}^2}{r^2} (J^2 - \bar{J}^2) - 2M(2J^2 - \bar{J}^2) - 4\bar{\Lambda} r^2 (J^2 + \bar{J}^2 - 2Mr^2) \right] \Big|_{r_{c.o.}}, \\ \mathcal{C} &= \left[4\bar{\Lambda}^2 r^8 + 2\bar{\Lambda} \bar{J}^2 r^4 + \frac{\bar{J}^2}{4} \right] \Big|_{r_{c.o.}}. \end{aligned} \quad (52)$$

Thus, the real solution of the quartic equation for $L_{c.o.}$ is

$$L_{c.o.}^2 = \left[\frac{\mathcal{B} - \sqrt{\mathcal{B}^2 - 4\mathcal{A}\mathcal{C}}}{2\mathcal{A}} \right] \Big|_{r_{c.o.}}, \quad (53)$$

and the energy is given by $E_{c.o.} = JL_{c.o.}/2r_{c.o.}^2 + \sqrt{\mathcal{F}(r_{c.o.}) + L_{c.o.}^2 \mathcal{F}(r_{c.o.})/r_{c.o.}^2}$. Also, it is possible to determine the periods of revolution of the circular orbits, both stable and unstable, with respect to the proper time τ , $T_\tau = 2\pi/\phi(r_{c.o.})$, and coordinate time t , $T_t = T_\tau t(r_{c.o.})$. Thereby, the period of a revolution according to the proper time is

$$T_\tau = \frac{4\pi(-\bar{\Lambda})r_{c.o.}(r_{c.o.}^2 - r_+^2)(r_{c.o.}^2 - r_-^2)}{J\sqrt{(r_{c.o.}^2 + L_{c.o.}^2)\mathcal{F}(r_{c.o.})} + 2L_{c.o.}r_{c.o.}\mathcal{F}(r_{c.o.})}, \quad (54)$$

and the period according to the coordinate time is

$$T_t = \frac{4\pi r_{c.o.}^2 \sqrt{(r_{c.o.}^2 + L_{c.o.}^2)\mathcal{F}(r_{c.o.})}}{J\sqrt{(r_{c.o.}^2 + L_{c.o.}^2)\mathcal{F}(r_{c.o.})} + 2L_{c.o.}r_{c.o.}\mathcal{F}(r_{c.o.})}. \quad (55)$$

On the other hand, Taylor expanding the effective potential around $r = r_S$, one can write $V(r) = V(r_S) + V'(r_S)(r - r_S) + \frac{1}{2}V''(r_S)(r - r_S)^2 + \dots$, where $'$ means derivative with respect to the radial coordinate. Obviously, in these orbits $V'(r_S) = 0$, so, by defining the *smaller* coordinate $x = r - r_S$, together with *the epicycle frequency* $\kappa^2 = V''(r_S)$ [20], we can rewrite the above equation as $V(x) \approx E_S + \kappa^2 x^2/2$ where E_S is the energy of the particle in the stable circular orbit. Also, it is easy to see that test particles satisfy the harmonic equation of motion $\ddot{x} = -\kappa^2 x$. Therefore, the epicycle frequency is given by

$$\kappa^2 = \frac{JL_{c.o.}}{r^4} \left[3 + \frac{r^4 \mathcal{F}'' + r^2 L_{c.o.}^2 \mathcal{F}'' - 4r \mathcal{F}' L_{c.o.}^2 + 6L_{c.o.}^2 \mathcal{F}}{r^3 \mathcal{F}' + r \mathcal{F}' L_{c.o.}^2 - 2L_{c.o.}^2 \mathcal{F}} - \frac{r^3 \mathcal{F}' + r \mathcal{F}' L_{c.o.}^2 - 2L_{c.o.}^2 \mathcal{F}}{2(r^2 \mathcal{F} + L_{c.o.}^2 \mathcal{F})} \right] \Big|_{r_S}. \quad (56)$$

C. Critical trajectories

There are two critical orbits that approach to the unstable circular orbit asymptotically. In the first kind, the particle arises from $r = r_A$, and in the second kind, the particle starts from a finite distance $r = r_i$ bigger than the horizon radius, but smaller than the unstable radius, see Fig. 7. By considering $\phi = t = \tau = 0$, and Eq. (22), the proper time for the critical orbit of first kind is

$$\tau(r) = -\frac{1}{(-\bar{\Lambda})^{1/2}} \int_{r_A}^r \frac{r^2 dr}{(r^2 - r_U^2) \sqrt{r_A^2 - r^2}}, \quad (57)$$

whose solution is given by

$$\tau(r) = \frac{1}{\sqrt{-\Lambda}} \left[\psi(r) + \frac{r_U}{\sqrt{r_A^2 - r_U^2}} \psi_U(r) \right], \quad (58)$$

where

$$\psi[r] = \tan^{-1} \sqrt{\frac{r_A^2}{r^2} - 1}, \quad (59)$$

and

$$\psi_U[r] = \tanh^{-1} \left[\frac{r_U}{r} \sqrt{\frac{r_A^2 - r^2}{r_A^2 - r_U^2}} \right]. \quad (60)$$

Now, for the critical trajectories of second kind the proper time is

$$\tau(r) = \frac{1}{\sqrt{-\Lambda}} \left[\psi(r) - \psi(r_i) + \frac{r_U [\psi_U(r) - \psi_U(r_i)]}{\sqrt{r_A^2 - r_U^2}} \right], \quad (61)$$

On the other hand, by considering $\phi = t = \tau = 0$, Eqs. (21) and (22) the coordinate time for the critical trajectory of first kind is

$$t(r) = - \int_{r_A}^r \frac{r^2 [Er^2 - JL/2] dr}{(-\bar{\Lambda})^{3/2} (r^2 - r_+^2)(r^2 - r_-^2)(r^2 - r_U^2) \sqrt{r_A^2 - r^2}}, \quad (62)$$

whose solution is

$$t(r) = \frac{1}{(-\bar{\Lambda})^{3/2}} \sum_{j=1}^3 \tilde{k}_j \psi_j(r), \quad (63)$$

where

$$\psi_1(r) = \frac{r_U}{\sqrt{r_A^2 - r_U^2}} \tanh^{-1} \left[\frac{r_U}{r} \sqrt{\frac{r_A^2 - r^2}{r_A^2 - r_U^2}} \right], \quad (64)$$

$$\psi_2(r) = \frac{r_+}{\sqrt{r_A^2 - r_+^2}} \tanh^{-1} \left[\frac{r_+}{r} \sqrt{\frac{r_A^2 - r^2}{r_A^2 - r_+^2}} \right], \quad (65)$$

$$\psi_3(r) = \frac{r_-}{\sqrt{r_A^2 - r_-^2}} \tanh^{-1} \left[\frac{r_-}{r} \sqrt{\frac{r_A^2 - r^2}{r_A^2 - r_-^2}} \right] \quad (66)$$

and

$$\tilde{k}_1 = \frac{Er_U^2 - JL/2}{(r_U^2 - r_+^2)(r_U^2 - r_-^2)}, \quad \tilde{k}_2 = -\frac{Er_+^2 - JL/2}{(r_U^2 - r_+^2)(r_+^2 - r_-^2)}, \quad \tilde{k}_3 = \frac{Er_-^2 - JL/2}{(r_U^2 - r_-^2)(r_+^2 - r_-^2)}. \quad (67)$$

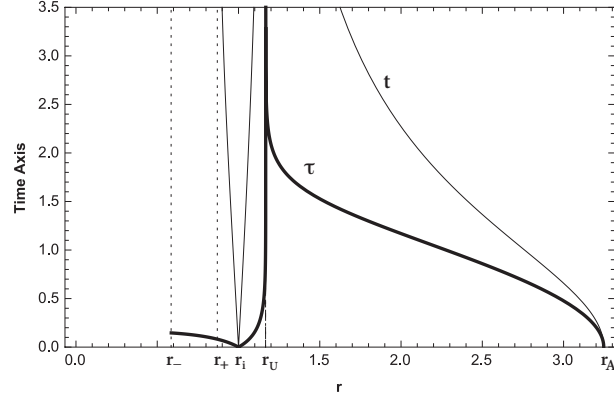


FIG. 7: The behaviour of the proper (τ) (thick line) and coordinate (t) (thin line) time as a function of r for critical trajectories of first and second kind with $M = a = b = \lambda = 1$, $\Lambda = -1$, $J = 1.2$, $\xi = 1.1$, $r_- \approx 0.59$, $r_+ \approx 0.87$, $r_i = 1.00$, $r_U \approx 1.17$, $r_A \approx 3.25$, and $E_U \approx 11.92$.

For the critical trajectories of second kind the coordinate time is

$$t(r) = \frac{1}{(-\bar{\Lambda})^{3/2}} \sum_{j=1}^3 \tilde{k}_j [\psi_j(r) - \psi_j(r_i)]. \quad (68)$$

In Fig. 7, we plot the behaviour of the proper and coordinate time as a function of r . We observe that for both times, the particle take an infinity time in to arrive to the unstable circular orbit. Finally, by using Eq. (20), and (22), the angular coordinate ϕ for the trajectories of first kind is

$$\phi_C(r) = \frac{1}{(-\bar{\Lambda})^{3/2}} \sum_{i=1}^3 \eta_i \psi_i(r), \quad (69)$$

where

$$\eta_1 = \frac{1}{(r_U^2 - r_+^2)(r_U^2 - r_-^2)} \left(\frac{E_u J}{2} - LM + (-\bar{\Lambda})L r_U^2 - \frac{L(J^2 - \bar{J}^2)}{4r_U^2} \right), \quad (70)$$

$$\eta_2 = \frac{-1}{(r_U^2 - r_+^2)(r_+^2 - r_-^2)} \left(\frac{E_u J}{2} - LM + (-\bar{\Lambda})L r_+^2 - \frac{L(J^2 - \bar{J}^2)}{4r_+^2} \right), \quad (71)$$

$$\eta_3 = \frac{1}{(r_U^2 - r_-^2)(r_+^2 - r_-^2)} \left(\frac{E_u J}{2} - LM + (-\bar{\Lambda})L r_-^2 - \frac{L(J^2 - \bar{J}^2)}{4r_-^2} \right). \quad (72)$$

While that for critical trajectories of second kind is

$$\phi_C(r) = \frac{1}{(-\bar{\Lambda})^{3/2}} \sum_{j=1}^3 \eta_j [\psi_j(r) - \psi_j(r_i)]. \quad (73)$$

In Fig. 8, we show the behavior of the angular coordinate as a function of r . We can observe that for both trajectories, first and second kind, the angular coordinate diverges at the unstable circular radius.

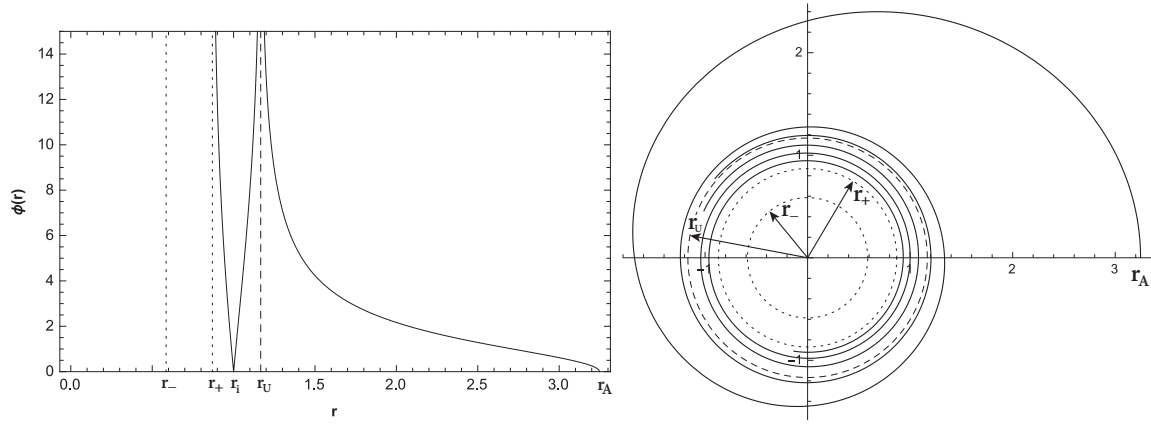


FIG. 8: Critical trajectory of first and second kind, for particles with $L = 12$, $M = a = b = \lambda = 1$, $\Lambda = -1$, $J = 1.2$, $\xi = 1.1$, $E_U = 11.92$, $r_- \approx 0.59$, $r_+ \approx 0.87$, and $r_i = 1.0$. For orbit of the first kind (thin line) the test particle arrived from $r_A = 3.25$, where $r_U \approx 1.17$ corresponds to the radius of the unstable circular orbit (dashed circle).

D. Radial motion

The radial motion corresponds to a trajectory with null angular momentum $L = 0$, and the particles, see Fig. 4, are destined to fall towards the event horizon. The effective potential Eq. (23) is $V(r) = \left(-M + \frac{\bar{J}^2}{4r^2} - \bar{\Lambda}r^2\right)^{1/2}$, and Eqs. (20), (21) and (22) yield

$$\dot{\phi} = -\frac{E J}{2\bar{\Lambda}(r^2 - r_+^2)(r^2 - r_-^2)}, \quad (74)$$

$$\dot{t} = -\frac{E r^2}{\bar{\Lambda}(r^2 - r_+^2)(r^2 - r_-^2)}, \quad (75)$$

$$\pm \dot{r} = \sqrt{E^2 + M - \frac{\bar{J}^2}{2r^2} + \bar{\Lambda}r^2}, \quad (76)$$

where the $(-)$ sign for \dot{r} , corresponds to particles falling into the event horizon, and the $(+)$ sign corresponds to particles that have a return point r_0 , for $E > E_+$, given by

$$r_0 = \sqrt{\frac{M + E^2}{-\bar{\Lambda}}} \sin \left[\frac{1}{2} \sin^{-1} \left(\frac{\bar{J}\sqrt{-\bar{\Lambda}}}{M + E^2} \right) + \frac{\pi}{2} \right]. \quad (77)$$

Now, choosing as initial conditions that the particle starts at $r = r_0$, and $\phi = t = \tau = 0$, the solution of Eq. (76) is

$$\tau(r) = \frac{1}{2\sqrt{-\bar{\Lambda}}} \left(\sin^{-1} \left[\frac{M + 2\bar{\Lambda}r^2 + E^2}{\sqrt{\bar{J}^2\bar{\Lambda} + (M + E^2)^2}} \right] - \sin^{-1} \left[\frac{M + 2\bar{\Lambda}r_0^2 + E^2}{\sqrt{\bar{J}^2\bar{\Lambda} + (M + E^2)^2}} \right] \right). \quad (78)$$

Also, a straightforward integration of Eqs. (75) and (76) leads to

$$t(r) = \frac{E}{2(-\bar{\Lambda})^{3/2}} \left[\frac{r_+^2}{\sqrt{p(r_+)}} \ln \left| \frac{r_0^2 - r_+^2}{r^2 - r_+^2} \cdot \frac{F_+(r)}{F_+(r_0)} \right| - \frac{r_-^2}{\sqrt{p(r_-)}} \ln \left| \frac{r_0^2 - r_-^2}{r^2 - r_-^2} \cdot \frac{F_-(r)}{F_-(r_0)} \right| \right], \quad (79)$$

where

$$F_{\pm}(r) = 2p(r_{\pm}) + \left(\frac{E^2 + M}{-\bar{\Lambda}} - 2r_{\pm}^2 \right) (r^2 - r_{\pm}^2) + 2\sqrt{p(r_{\pm})}\sqrt{P_{\pm}(r)}, \quad (80)$$

$$p(r) = -r^4 + \frac{E^2 + M}{-\bar{\Lambda}}r^2 - \frac{\bar{J}^2}{4(-\bar{\Lambda})}, \quad (81)$$

$$P_{\pm}(r) = p(r_{\pm}) + \left(\frac{E^2 + M}{-\bar{\Lambda}} - 2r_{\pm}^2 \right) (r^2 - r_{\pm}^2) - (r^2 - r_{\pm}^2)^2. \quad (82)$$

In Fig. 9, we show the behaviour of the proper and coordinate time as a function of r , we can observe that the particle arrives to the event horizon in a finite proper time, and infinite coordinate time. Finally, the solution for the angular coordinate ϕ is

$$\phi(r) = \frac{E J}{4(-\bar{\Lambda})^{3/2}} \left[\frac{1}{\sqrt{p(r_+)}} \ln \left| \frac{r_0^2 - r_+^2}{r^2 - r_+^2} \cdot \frac{F_+(r)}{F_+(r_0)} \right| - \frac{1}{\sqrt{p(r_-)}} \ln \left| \frac{r_0^2 - r_-^2}{r^2 - r_-^2} \cdot \frac{F_-(r)}{F_-(r_0)} \right| \right], \quad (83)$$

where we have used Eq. (74) and Eq. (76). In Fig. 10, we plot the behaviour of the angular coordinate, where we observe that the angular coordinate becomes infinity at the event horizon.

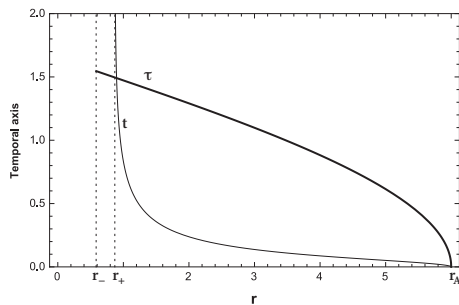


FIG. 9: The behaviour of the coordinate time (t) and the proper time (τ) along an unbounded time-like radial geodesic described by a test particle, starting at $r_0 = 6$ and falling towards the singularity, for $L = 0$, $M = a = b = \lambda = 1$, $\Lambda = -1$, $E = 5.63$, $J = 1.2$, $\xi = 1.1$, $r_+ \approx 0.87$, and $r_- \approx 0.59$.

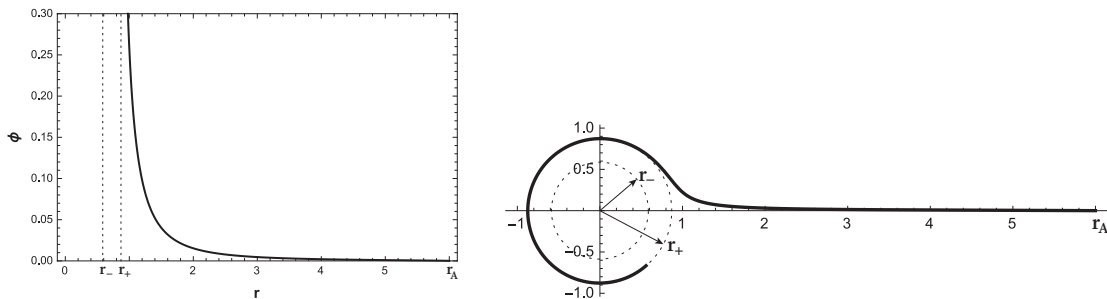


FIG. 10: The behavior of the coordinate $\phi(r)$, starting at $r_0 = 6$ and falling towards the singularity with $L = 0$, $M = a = b = \lambda = 1$, $\Lambda = -1$, $J = 1.2$, $\xi = 1.1$, $r_- \approx 0.59$ and $r_+ = 0.87$. In the polar plot, the trajectory approaching the horizon will spiral around the black hole an infinite number of times.

V. REMARKS AND CONCLUSIONS

In this work, we studied the motion of particles in the background of a rotating three-dimensional Hořava AdS black hole described by a Lorentz-violating version of the BTZ black hole, and we calculated the time like geodesics, which possess a rich structure and allow different kinds of trajectories for the particles. This work along with the null geodesic described in Ref. [10], complete the geodesic structure for the rotating three-dimensional Hořava AdS black hole. We have shown the existence of planetary orbits, where we have obtained an exact solution and we have determined the periods of revolution. Also, circular orbits, where we have shown the existence of the stable and unstable circular orbits, and we determined the periods of revolution, as well as, the epicycle frequency for the stable circular orbit. Also, critical orbits of first and second kind that approach to the unstable circular orbit asymptotically, and finally the radial trajectories which are all bounded. However, their counterpart, i.e, the BTZ metric allow only the radial trajectory; thereby, the differences observed with respect to the BTZ metric could be attributed to the breaking of the Lorentz invariance.

Therefore, the Lorentz-violating version of the BTZ black hole, turn on an effective potential with a more rich structure allowing different kind of orbits. As it was shown [10], for photons new kinds of orbits are allowed, such as unstable circular orbits and trajectories of first kind. While that for particles the planetary and circular orbits are allowed, which does not occur in the BTZ background. In this way, the breaking of the Lorentz invariance could generate orbits that could not occur in invariant Lorentz theories.

Acknowledgments

Y.V. acknowledge support by the Dirección de Investigación y Desarrollo de la Universidad de La Serena, Grant No. PR18142.

-
- [1] M. Banados, C. Teitelboim and J. Zanelli, *Phys. Rev. Lett.* **69** (1992) 1849 [hep-th/9204099].
 - [2] S. Carlip, *Class. Quant. Grav.* **12**, 2853 (1995) [gr-qc/9506079].
 - [3] C. Farina, J. Gamboa and A. J. Segui-Santonja, *Class. Quant. Grav.* **10**, L193 (1993) [gr-qc/9303005].
 - [4] N. Cruz, C. Martínez and L. Pena, *Class. Quant. Grav.* **11**, 2731 (1994) [gr-qc/9401025].
 - [5] T. P. Sotiriou, M. Visser and S. Weinfurtner, *Phys. Rev. D* **83**, 124021 (2011) [arXiv:1103.3013 [hep-th]].
 - [6] T. P. Sotiriou, I. Vega and D. Vernieri, *Phys. Rev. D* **90**, no. 4, 044046 (2014) [arXiv:1405.3715 [gr-qc]].
 - [7] P. Horava, *Phys. Rev. D* **79**, 084008 (2009) [arXiv:0901.3775 [hep-th]].
 - [8] R. Bécar, P. A. González, E. Papantonopoulos and Y. Vásquez, *Eur. Phys. J. C* **80**, no. 7, 600 (2020) [arXiv:1906.06654 [gr-qc]].
 - [9] R. Bécar, P. A. González and Y. Vásquez, arXiv:2002.04421 [gr-qc].
 - [10] P. A. González, M. Olivares, E. Papantonopoulos and Y. Vásquez, *Phys. Rev. D* **101**, no. 4, 044018 (2020) [arXiv:1912.00946 [gr-qc]].
 - [11] S. Fernando, D. Krug and C. Curry, *Gen. Rel. Grav.* **35**, 1243 (2003).
 - [12] N. Cruz, M. Olivares and J. R. Villanueva, *Eur. Phys. J. C* **73**, 2485 (2013) [arXiv:1305.2133 [gr-qc]].
 - [13] S. Kazempour and S. Soroushfar, *Chin. J. Phys.* **65**, 579 (2020) [arXiv:1709.06541 [gr-qc]].
 - [14] G. Panotopoulos, *Gen. Rel. Grav.* **52**, no. 6, 54 (2020).
 - [15] T. Jacobson, *Phys. Rev. D* **81**, 101502 (2010) Erratum: [*Phys. Rev. D* **82**, 129901 (2010)] [arXiv:1001.4823 [hep-th]].
 - [16] B. Cropp, S. Liberati, A. Mohd and M. Visser, *Phys. Rev. D* **89**, no. 6, 064061 (2014) [arXiv:1312.0405 [gr-qc]].
 - [17] T. Zhu, Q. Wu, M. Jamil and K. Jusufi, *Phys. Rev. D* **100**, no. 4, 044055 (2019)
 - [18] Chandrasekhar S.: *The Mathematical Theory of Black Holes*. Oxford University Press, New York (1983).
 - [19] N. Deruelle and R. Ruffini, *Phys. Lett.* **52B**, 437 (1974).
 - [20] J. Ramos-Caro, J. F. Pedraza and P. S. Letelier, *Mon. Not. Roy. Astron. Soc.* **414**, 3105 (2011) [arXiv:1103.4616 [astro-ph.EP]].